JOURNAL OF NEUROTRAUMA
Volume 14, Number 1, 1997
Mary Ann Liebert, Inc.

Quantitative MRI of the Gray–White Matter Distribution in Traumatic Brain Injury

R.W. THATCHER,[1,2,3] M. CAMACHO,[1] A. SALAZAR,[4] C. LINDEN,[3] C. BIVER,[1] and L. CLARKE[3]

ABSTRACT

Quantitative analyses were performed on magnetic resonance images (MRIs) obtained from the brains of 31 traumatic brain-injured (TBI) patients and 25 normal control subjects. The quantitative analyses involved comparisons of the shapes of proton density gray scale pixel histograms obtained from both 3-mm and 5-mm slice thickness. Image segmentation was accomplished by a multispectral fuzzy C-means and/or k-nearest-neighbor (kNN) algorithms and manual classification was used to label segmented classes into CSF, white matter, gray matter, and other. Shape descriptors were derived from the pixel intensity histograms of the combined gray matter and white matter classes for each MRI slice. Statistical analyses revealed significant differences in pixel intensity distributions between TBI and control subjects. Normal control subjects tended to exhibit bimodal gray matter–white matter histograms, whereas, TBI patients tended to exhibit unimodal gray matter–white matter histograms. In the control subjects the pixels intermediate in intensity between gray and white matter were located primarily at the border between the gray and white matter, whereas TBI patients exhibited a thickening of the number of intermediate pixels at the border as well as an increase in intermediate pixels in the middle of the gray and white matter. The greater the severity of TBI, then the larger the number of intermediate intensity pixels within and between gray and white matter. Further analyses demonstrated shifts in magnetic resonance relaxation times in gray and white matter in TBI patients, which suggested that the tendency toward unimodality in TBI patients represents a pathological reduction in brain differentiation due to measurable biophysical change.

Key words: quantitative MRI; pixel intensity change; traumatic brain injury

INTRODUCTION

CURRENTLY, CLINICAL MRI evaluation of human traumatic brain injury (TBI) involves visual examination using both short TR/TE and long TR/short TE as well as T2* visual examinations for the presence of hemosiderin (Gentry, 1990). Quantitative MRI analyses in TBI patients typically involves morphometric measurements of specific brain regions such as the volume of the ventricles (Johnson et al., 1994; Prayer and Gean, 1994), size of the temporal horn and hippocampus (Bigler et al., 1996; Gale et al., 1994), or white matter hyperintensities and gray–white ratios (Gentry et al., 1988; Gentry, 1994). However, all of these MRI measures are relatively insensitive and nonspecific with detection accuracies ranging between 10% and approximately 40% in the hands

[1]Bay Pines Veterans Administration Medical Center, [2]Department of Neurology and [3]Radiology, University of South Florida College of Medicine, Tampa, Florida 33612.
[4]Defense and Veterans Head Injury Program, Washington D.C.

of experienced neuroradiologists (Gentry, 1990, 1994). Diffuse axonal injury (DAI) is one of the most common types of injury in severe head trauma (Strich, 1956, 1961; Adams et al., 1982; 1989; Gennarelli et al., 1982), constituting approximately 48% of all primary lesions (Gentry et al., 1988). DAI is visually identified in MRI studies by multiple, small, focal lesions scattered throughout the white matter. Most such lesions are located at the gray–white matter boundary, which is not an unexpected location for shear injury given the different densities between gray and white matter. DAI lesions are typically nonhemorrhagic in nature, range in size from 5 to 15 mm, and are usually ovoid to elliptical in shape (Gentry et al., 1990). Autopsy and histopathological studies have shown that the extent of axonal injury always exceeds that visualized by MRI analyses (Strich, 1956, 1961; Adams et al., 1982, 1989; Gentry, 1990, 1994). As concluded by Gentry (1990), visual examination by MRI greatly underestimates the true extent of DAI and detects only regions of DAI where axonal disruption is extensive.

Groswasser et al. (1987), in a visual examination study of MRIs, reported a blurring or reduced contrast between gray and white matter in TBI patients. However, to our knowledge, there are no published studies of quantitative MRI analyses of gray matter–white matter differentiation in TBI patients. An objective and quantitative MRI analysis of TBI and brain damage in general could be of clinical value and serve as an adjunct to conventional neuroradiological visual examination. The goal of the present study is to explore an approach to quantitative MRI analyses of gray matter–white matter differentiation in TBI patients in an effort to extend the usefulness of MRI in the detection of brain abnormalities. Our approach consisted of three steps: (1) segment and differentiate gray matter and white matter cortical tissue from cerebral spinal fluid (CSF) in normals and TBI patients, (2) develop normalized histograms of gray matter and white matter pixel intensities in different slices, and (3) compare the slice by slice shapes of the gray matter–white matter pixel intensity histograms between normals and TBI patients.

Our working hypothesis is that TBI results in a reduction in gray–white matter differentiation and such a reduction can be quantified using histogram shape analysis. Specifically, it is hypothesized that MRI proton density histograms of gray matter and white matter should exhibit a bimodal distribution in normal individuals, while the gray–white matter histogram in TBI patients should be less bimodal or even unimodal. The goal is to explore the use of quantitative measures of MR pixel intensity histograms for the diagnosis and detection of brain injury.

METHODS

Patients

A total of 31 traumatic brain-injured patients were included in the study. Twenty-three patients were from the James A. Haley VA hospital and 8 were from the Walter Reed Army Medical Center as part of the Defense and Veterans Head Injury Program (DVHIP). Of the 35 patients, 34 were males. The patients ranged in age from 19 to 60 with a mean age of 32 and SD = 11.3. The time between injury and MRI testing ranged from 2 days to 5 years and 3 months with a mean interval of 440 days and an SD = 850.5 days. Only closed head-injured patients were included in the study. Mild, moderate, and severe TBI was defined based upon the following criteria: mild ($N = 7$) loss of consciousness (LOC) 0 to 29 min, posttraumatic amnesia (PTA) <24 h, and Glasgow Coma Score (GCS) between 13 to 15; moderate ($N = 11$) LOC >30 min and <24 h, PTA >24 h and <1 week, and GCS >9 to 12; severe ($N = 13$) LOC = >24 h, PTA >1 week, and GCS <8. All of the patients were diagnosed using ICD-9 (i.e., Intracranial Injury Excluding those with penetrating head wounds or codes within the 850 to 854 categories). Approximately 60% of the patients were motor-vehicle accident (MVA) victims, 10% were pedestrians, and the remainder were victims of industrial or home accidents (20%) or violent crime (10%).

Normal Controls

A total of 25 normal control subjects (18 males, age range 22 to 36 and mean age = 32.36 and SD 4.43) were included in the study. The MRIs from 23 normals were obtained at the University of South Florida College of Medicine and two normal subjects were imaged at the James A. Haley VA. The normal subjects were all medical students and/or graduate students without a history of traumatic brain injury.

MRI Acquisition

The MRI scans of the 12 patients located at Walter Reed Army Medical Center were acquired on a G.E. Signa 1.5 T scanner using three different sequences: (1) double-echo for T2 and proton density and (2) a T1-weighted sequence. All acquisitions used 5-mm slices and no gap sequences. The proton density and T2 sequences had a TR = 2500 msec with TEs of 20 and 80 msec, FOV of 20 cm, a 90° flip angle, and a 256 × 192 matrix. The T1-weighted sequence used TR = 600 msec with a TE = 20 msec, FOV = 20 cm, a 90° flip angle, and a 256 × 192 matrix.

MR images of 23 normal controls from the University

of South Florida College of Medicine were acquired also on a G.E. Signa 1.5 T scanner with 5-mm slice thickness and no gap sequences. The proton density and T2 sequences had a TR = 3000 msec with TEs of 16 and 17 msec for (PD), and 96 and 102.2 msec for T2, FOV of 24 cm, a 90° flip angle, and a 256 × 192 matrix. The T1-weighted sequence used TR = 500 msec with a TE = 27 msec, FOV = 24 cm, a 90° flip angle, and a 256 × 192 matrix.

The MR images of 23 TBI patients and 2 normal controls were acquired at the James A. Haley VA Hospital on a Picker 1.5T scanner with 3-mm slice thickness and no gap sequences. The proton density and T2 sequences had a TR = 3000 msec with TEs of 30 and 90 msec, FOV of 24 cm, a 90° flip angle, and a 256 × 192 matrix. The T1-weighted sequence used TR = 883 msec with a TE = 20 msec, FOV = 24 cm, a 90° flip angle, and a 256 × 192 matrix.

Image Segmentation and Classification

A multispectral k-nearest neighbor (kNN) manual segmentation and classification algorithm (Clarke et al., 1994) was used for studies of absolute pixel intensity shifts and machine parameter comparisons. For gray matter and white matter histogram analyses, a multispectral fuzzy c-means (FCM) algorithm was used (Hall et al., 1992; Bezdek et al., 1993; Clarke et al., 1995). This involved the use of a brain mask that was manually traced for each axial MR proton density image via a polygon tracing algorithm isolating the brain from skull and dura. To minimize error and to improve segmentation accuracy a validity-guided reclustering (VGC) algorithm was used on each FCM segmented slice (Bensaid et al., 1994; Clarke et al., 1995). Every segmented slice was manually classified via a graphical-user interface into 5 classes: background, white matter, gray matter, CSF, and other. All subsequent analyses involve grayscale histograms of pixels identified as members of the combined white matter and gray matter class.

Different numbers of slices were analyzed depending on slice thickness. For the G.E. 5 mm Signa studies a total of 9 slices were analyzed while 15 slices were analyzed for the Picker 3 mm MRI studies. This resulted in the same vertical span of 4.5 cm to be studied independent of the type of MRI machine or slice thickness. The selection of the first axial slice was the same for all patients and normals. The lowest and starting slice was identified at the level of the genu of the corpus callosum, septum pellucidum, and the forceps major and minor. Figure 1 shows a representative example of the starting slice anatomical landmarks. In the figures and tables below, a set of 9 slices were selected from the Picker studies to correspond to the 9 slices from the G.E. studies for purposes of statistical analyses. The selected Picker slices

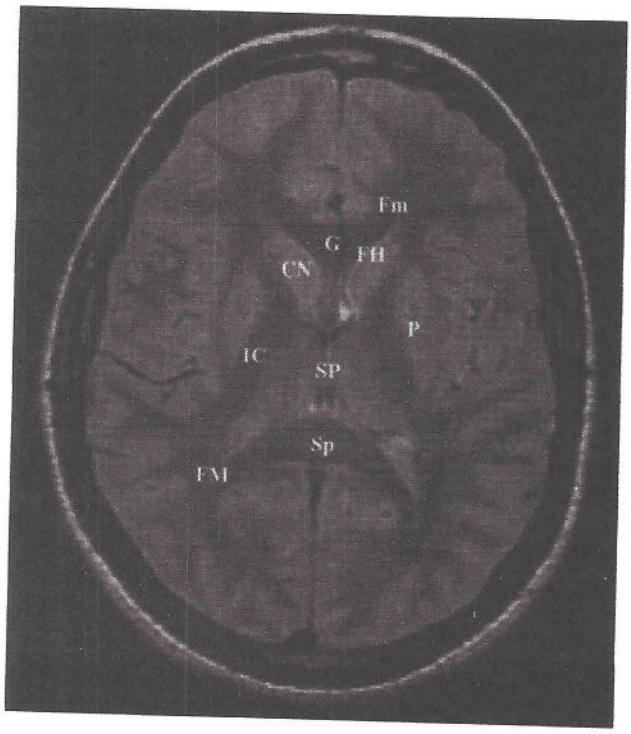

FIG. 1. A representative example of the first or lowest slice and the anatomical landmarks by which similar first slices were selected for all subjects in the study. Nine 5-mm G.E. slices and 15 3-mm Picker slices spanning a total of 4.5 cm of the brain were analyzed, starting with this first reference slice. Anatomical landmarks: Fm, forceps minor; G, genu of the corpus callosum; FH, frontal horn of the lateral ventricles; CN, caudate nucleus; P, putamen; IC, internal capsule; SP, septum pellucidum; Sp, splenium of the corpus callosum; FM, forceps major.

were 1, 3, 5, 7, 8, 9, 10, 13, and 15. The remaining four Picker MRI slices were analyzed, but not statistically compared to the G.E. MRI slices.

Pixel Intensity Histograms

After segmentation and classification of CSF, white matter and gray matter, histograms of the combined class of gray and white matter pixel intensities were computed for each proton density slice with pixel intensity on the abscissa (x-axis) and frequency counts on the ordinate (y-axis). No attempt was made to bin the data, rather the distributions of raw pixel values were plotted for each slice. To normalize pixel intensity histograms obtained from different MRI scanners, a linear Z transform of the pixel intensity distributions was computed. This involved, for each histogram, computing the mean and standard deviation of pixel intensity, subtracting the mean from each individual pixel and dividing by the standard deviation. To eliminate noisy pixels only the ranges of

pixel intensities between ±4 SD were included in the analyses.

Smoothing and First Derivative Computations

To smooth and condition the histograms of gray matter–white matter pixel intensity the histograms were filtered using a Savitzky–Golay procedure (Savitzky and Golay, 1964). Since the hypothesis was the detection of bimodal and/or unimodal peaks, a fourth order filter was used in which the full width of the filter was between 1 and 2 times the full width at half maximum (FWHM) of the pixel histogram (Press et al., 1994). The FWHM was estimated by setting the width of the filter equal to 1.5 standard deviations (i.e., ±0.75 SD) of the histogram. Visual examination of the fourth-order filter showed that this was a good estimate resulting in minimal distortion and no loss of resolution. Figure 2 shows the raw normalized pixel histograms with the superimposed smoothed Savitzky–Golay values of a slice from a representative normal control and a representative TBI patient.

The first derivative of the pixel histograms (Fig. 2b and d) was computed in order to identify the presence or absence of bimodality and to quantify peak area of the second positive first derivative (SPFD). The presence of bimodality was signaled by the presence of a second positive first derivative as shown in Figure 2. A second positive first derivative (SPFD) was present if two criteria were met: (1) two distinct and positive first derivatives must be present and (2) the second positive first derivative value represented a peak as defined by a 13 point positive maximum. Although a automatic computer program was used for identification of a second positive first derivative, all pixel intensity histograms and first derivative curves were also visually examined to ensure that there were no errors. The above two criteria were found to accurately detect a bimodality in the pixel intensity histograms.

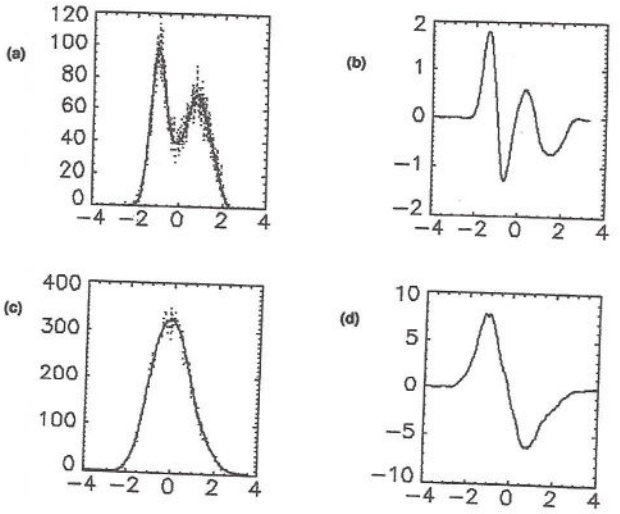

FIG. 2. (a,c) The raw normalized pixel histograms with the superimposed smoothed Savitzky–Golay values from a normal control and a TBI patient, respectively. (b,d) The first derivatives computed from a and c using the Savitzky–Golay procedure. These histograms and smoothed curves were typical of the subjects in this study and show no distortion or loss of resolution, while demonstrating clear differences in histogram shapes and the presence of a bimodality as evidenced by the occurrence of a second positive first derivative (SPFD) in the control and an absence of bimodality as evidenced by the lack of an SPFD in the TBI patient.

SPFD Peak Area

The peak area of the second positive first derivative was calculated for all slices and all subjects. The area of the second positive first derivative was calculated by summing the pixel intensity values within the region defined as the zero crossing points to the left and right of the SPFD peak. To normalize the second positive first derivative values across MRI machines and slice thickness, the area of the second positive first derivative peak was calculated as a percentage of the total first derivative values (±4 SD). If a second positive first derivative was absent then a score of 0 was entered for peak area.

Skewness and Kurtosis

The statistical moments of skewness and kurtosis were also computed for the pixel distributions of each subject and each slice. Skewness was defined as

$$M_1 = \frac{n^{1/2}\sum_{i=1}^{n}(X_i - \bar{X})^3}{\left[\sum_{i=1}^{n}(X_i - \bar{X})^2\right]^{3/2}}$$

and Kurtosis was defined as

$$M_2 = \frac{n\sum(X_i - \bar{X})^4}{\left[\sum(X_i - \bar{X})^2\right]^2} - 3$$

Intermediate Intensity Pixels

Two different methods were used to identify the intermediate intensity pixels: (1) the absolute number and percentage of pixels within ±0.125 SD of the mean of the pixel intensity histograms and (2) ±0.125 SD of the mean of the unimodal pixel intensity histograms and the minimum of the bimodal pixel intensity histograms. The anatomical location of the pixels within ±0.125 SD of the mean was determined by coloring the pixels as yellow and then visually examining each slice. This procedure was generally accurate since the mean was always very close if not

precisely at the maximum of the unimodal distributions. However, in the case of bimodal distributions the mean could be slightly to the left or right of the minimum or trough of the distribution. Thus, a second procedure was developed and compared to the first in which the precise minimum or trough of each bimodal distribution was identified and the pixel intensities at the minimum ±0.125 standard deviations were colored yellow and placed into the original MRI slices. There were no significant differences in these two methods, however, for accuracy the mean (±0.125 SD) was used for unimodal distributions and the number and percentage of pixels at ±0.125 SD of the minimum or trough of the bimodal distributions were used.

RESULTS

Presence or Absence of Bimodality in TBI Patients and Normals

Figure 3 shows examples of differences in slice by slice pixel intensity distributions in two representative normal controls obtained from the G.E. Signa MRI machine (two left columns) and two representative TBI patients (two right columns) also obtained on a G.E. Signa machine. Although most normal controls exhibited bimodality in all slices, Figure 3 shows a common finding of strong bimodality in the upper and lower range of slices. A similar but weaker bimodality was occasionally present in TBI patients as shown in the last column of Figure 3.

Similar differences in the slice by slice pixel intensity distributions occurred in the normal controls and TBI patients acquired by the 1.5T Picker MRI machine.

Tables 1 and 2 show the slice-by-slice distribution of bimodality in normal controls and TBI patients acquired on the 5-mm slice thickness G.E. Signa in Table 1 and from the 3-mm slice thickness Picker in Table 2. It can be seen that the strength and frequency of bimodality were significantly weaker in the TBI patients than in the controls for both the G.E. and Picker MRI machines. A Friedman nonparametric analysis of variance for the presence of a second positive first derivative for the two groups of subjects (TBI versus normal controls) was statistically significant for both the G.E. ($p < 0.0003$) and Picker MRI machines ($p < 0.001$).

Differences in SPFD Peak Area between TBI Patients and Normal Controls

Figure 4 shows the slice by slice mean peak area of the second positive first derivative (SPFD) in the combined G.E. and Picker normal controls and the TBI patients. A clear separation in mean values between normals and TBI patients is present for mean peak area and *t* tests showed a statistically significant overall *t* test ($T = 22.675$, $p < 0.00001$). All of the slices were statistically different except for slice 5 (range: $p < 0.02$ to $p < 0.0000001$). Analyses showed that statistically significant differences between the controls and TBI patients occurred independent of which MRI machine and slice thickness was used to acquire the data. For example, analyses showed a statistically significant main effect between TBI patients versus normals for both the G.E. (SPFD area, $T = 21.518$; $p < 0.00001$) and the Picker (SPFD area, $T = 10.22$; $p < 0.0001$).

Differences in Skewness and Kurtosis between TBI Patients and Normal Controls

The binomial measure of the presence or absence of bimodality is a limited analysis that does not allow for a deeper understanding of the underlying imaging differences between groups. A simple method to explore the differences between groups is to derive and compare histogram shape descriptors such as skewness and kurtosis (defined in the methods section). Mathematically, unimodality is more kurtotic and less skewed than bimodality. Thus, these measures of statistical moments can help quantify differences in pixel distributions in each MRI slice.

Figure 5 shows the mean skewness for the normal controls and TBI patients in the study (i.e., combined G.E. and Picker, $T = 12.83$, $p < 0.001$). It can be seen that skewness varies as a function of slice level and is different between normal controls and TBI patients. Statistical analyses revealed significant differences between TBI and controls for both the G.E. MRI machine ($T = 12.15$, $p < 0.001$) and the Picker MRI machine ($T = 2.18$, $p < 0.04$). Individual *t* test analyses showed that slices 3 to 5 were significantly different for normal controls versus TBI patients for the G.E. MRI study and slices 4 to 8 were significantly different for normal controls versus TBI patients for the Picker MRI study.

Figure 6 shows the mean kurtosis for the normal controls and TBI patients in the study (i.e., combined G.E. and Picker). It can be seen that kurtosis is relatively invariant of slice level and is different between normal controls and TBI patients, independent of MRI machine. Analyses showed statistically significant overall *t* values for both 5-mm slice thickness ($T = -68.264$, $p < 0.00001$) and 3-mm slice thickness ($T = -32.157$, $p < 0.00001$). Individual *t* test analyses showed that all slices ($p < 0.01$) within the 4.5 cm volume were significantly different between normal controls versus TBI patients, independent of slice thickness and MRI machine type.

Anatomical Distribution and Numbers of Intermediate Pixel Intensities

The previous analyses showed that TBI patients exhibited a more unimodal MRI pixel distribution than TBI

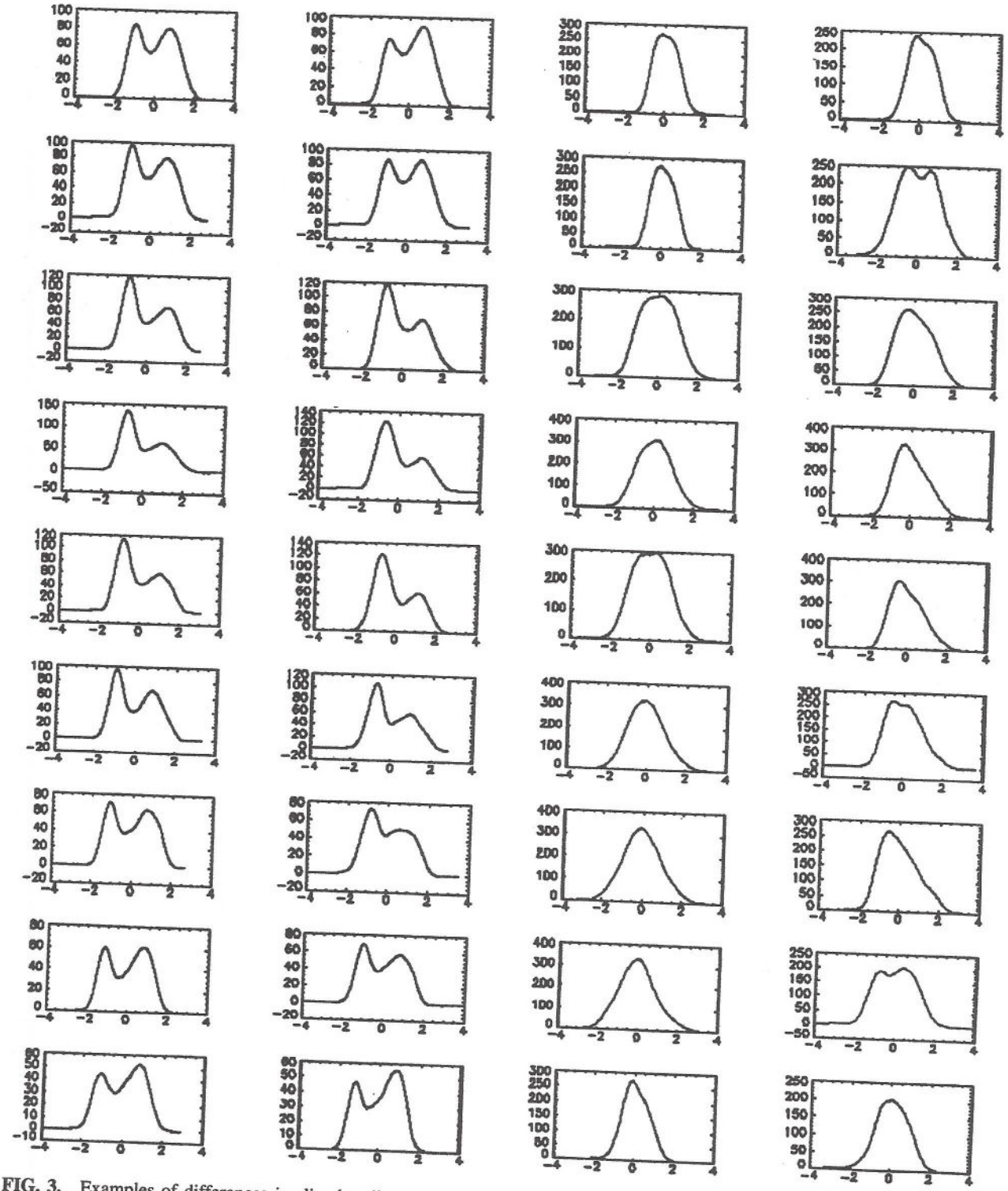

FIG. 3. Examples of differences in slice by slice pixel distributions in two representative normal controls obtained from the G.E. Signa MRI machine (two left columns) and two representative TBI patients (two right columns) also obtained on a G.E. Signa machine.

patients. This indicates that there are more pixel intensities intermediate to gray and white matter in TBI patients than in normals. The anatomical location and distribution of the intermediate pixel intensities were then visually evaluated by coloring them yellow in the original MRI slices. Analyses of variance revealed a statistically

TABLE 1. PERCENTAGE OF BIMODAL HISTOGRAM DISTRIBUTIONS FROM THE G.E. MRI

	Slice number								
	1	*2*	*3*	*4*	*5*	*6*	*7*	*8*	*9*
Control	88	96	96	92	96	100	100	100	96
TBI	33	28	20	18	27	33	50	59	32

significant increased number of intermediate intensity pixels in TBI patients compared to controls ($T = 56.257$, $p < 0.00001$) as well as a significant increase in the percentage of total pixels that were intermediate in intensity ($T = 97.828$, $p < 0.00001$). A systematic increase in the number and location of yellow or intermediate pixels was observed to occur as a function of the severity of TBI. Figure 7 shows examples of the distribution of yellow pixels in a normal subject (7a), a mild TBI patient (7b), a moderate TBI patient (7c), and a severe TBI patient (7d). In normal subjects (7a) the yellow pixels formed a pencil-like distribution at the border between gray and white matter. In mild TBI patients (7b) the yellow pixels formed a thicker border with a few yellow pixels in the gray and white matter; in moderate TBI patients (7c) the yellow pixels formed a thicker border and more scattered yellow pixels appeared in the gray and white matter. In severe TBI patients (7d) the yellow pixels formed an even thicker border and were widely distributed throughout the gray and white matter.

Reduced Gray-White Matter Differentiation and Pixel Intensity Shifts Underlying Histogram Changes

To further normalize and control for MRI machine differences gray matter and white matter intensities were compared to a stable reference such as the masseter muscle. Muscle is a good choice for a reference because its relaxation properties are essentially invariant across individuals and even across phylogeny (Bottomley et al., 1984). Therefore, the absolute intensity ratios between gray matter/muscle and white matter/muscle were computed and compared. The proton density (PD), T1 and T2 MR images from an arbitrarily selected subset of 10 normals acquired on the G.E. Signa (5-mm slice thickness) and 10 TBI patients also acquired on a G.E. Signa (5-mm slice thickness) were segmented and classified into white matter, gray matter, and masseter muscle using kNN segmentation (Clarke et al., 1994). Figure 8 shows examples of proton density intensities for the various tissue classes in three representative normals (left column) and three representative TBI patients (right column). A visually detectable shift in proton density toward higher gray and white matter pixel intensities, relative to muscle, was noted in TBI patients in comparison to normals.

Figure 9 shows the mean pixel intensity ratios between gray matter and muscle and white matter and muscle in PD, T1, and T2 images. Statistical analyses show that PD and T2 exhibit statistically significant differences between gray and white matter ratios in normals versus TBI patients (ranged from $p < 10^{-2}$ to $p < 10^{-5}$) with TBI patients showing a relative increase in gray matter and white matter pixel intensity in comparison to controls. In contrast, T1 failed to show statistically significant differences between normals and TBI patients. Further, in T1 there was a reversal of the direction of the ratio with gray matter and white matter in TBI patients exhibiting a decreased pixel intensity with respect to controls.

DISCUSSION

MRI Pixel Intensity Change (PIC) in TBI Patients

The results of this study consistently demonstrated a difference in the gray matter and white matter proton density pixel intensity distributions between normal subjects and traumatic brain-injured (TBI) patients. The TBI patients exhibited less bimodality and, thus, more unimodal distributions than did the normal control subjects as evidenced by the presence or absence of bimodality, SPFD peak area, and measures of skewness and kurtosis. In addition, a continuum of intermediate intensity pixels and unimodality was related to the severity of brain trauma. These differences were independent of 3-mm vs. 5-mm slice thickness and MRI scanner.

In a heterogeneous tissue such as the brain, partial volume effects are always present. However, in spite of partial volume effects or slight variations in machine para-

TABLE 2. PERCENTAGE OF BIMODAL HISTOGRAM DISTRIBUTIONS FROM THE PICKER MRI

	Slice number														
	1	*2*	*3*	*4*	*5*	*6*	*7*	*8*	*9*	*10*	*11*	*12*	*13*	*14*	*15*
Control	50	100	50	50	0	0	100	100	100	100	100	100	100	50	50
TBI	22	43	13	13	4	4	22	35	48	52	57	48	48	30	22

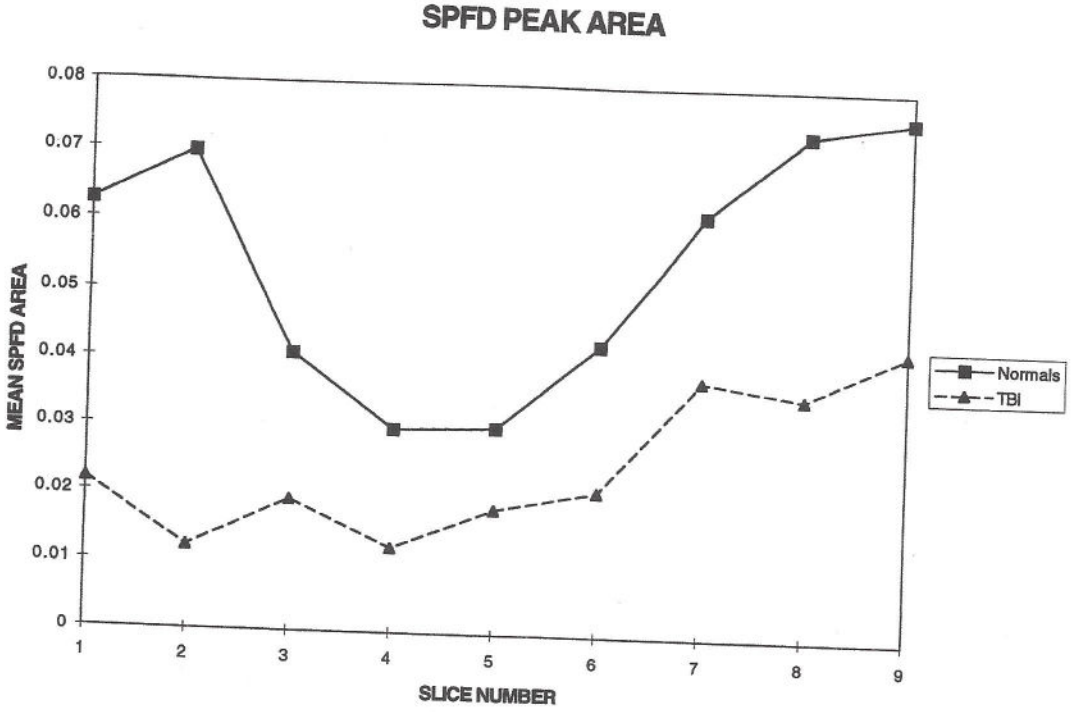

FIG. 4. The slice by slice mean peak area of the second positive first derivative (SPFD) for the combined G.E. and Picker studies of normal controls (solid lines) and TBI patients (dashed lines).

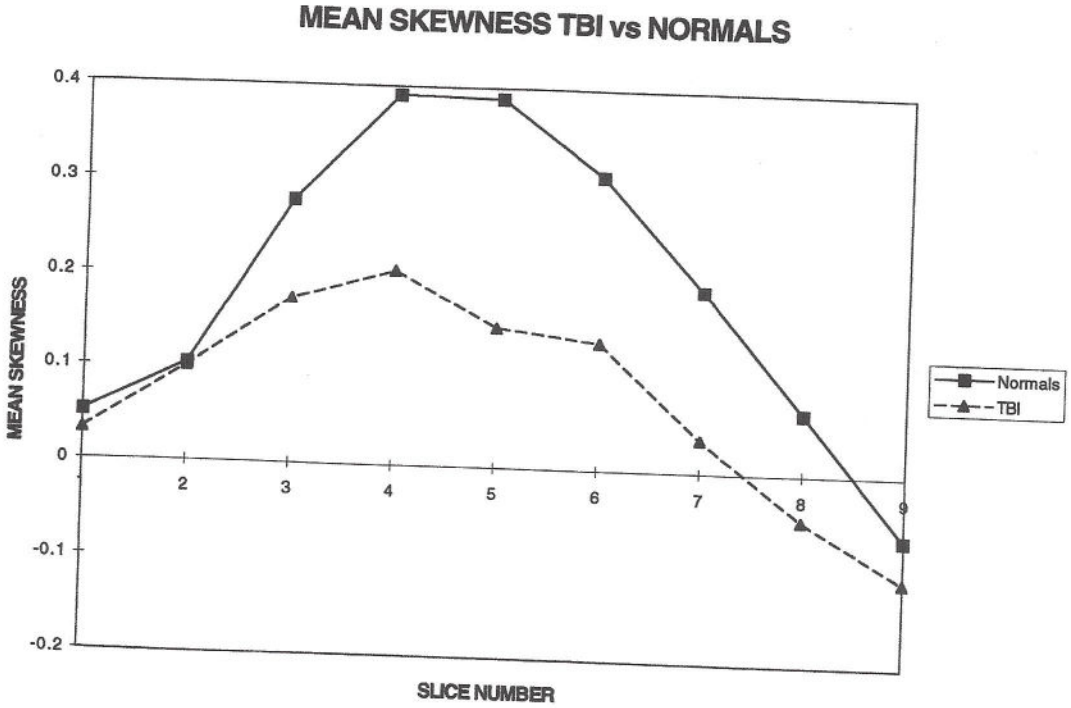

FIG. 5. Slice by slice mean skewness for the combined G.E. and Picker studies of normal controls (solid lines) and TBI patients (dashed lines).

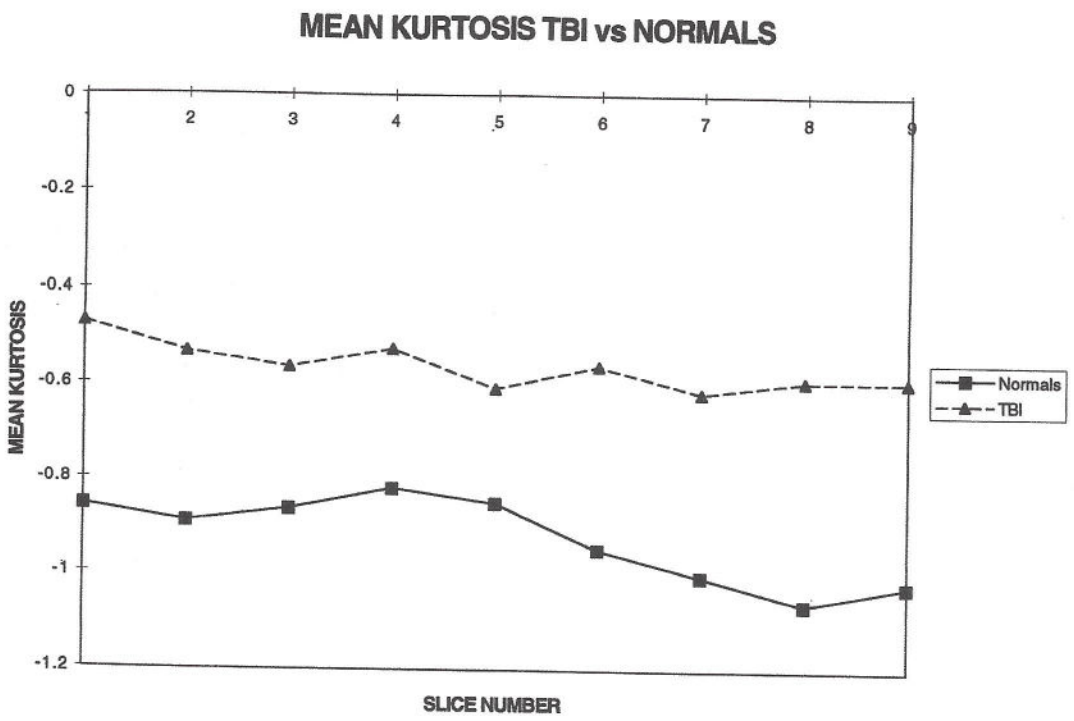

FIG. 6. Slice by slice mean kurtosis for the combined G.E. and Picker studies of normal controls (solid lines) and TBI patients (dashed lines).

meters, a bimodal distribution of pixel intensities is the expected distribution in proton density images of a healthy individual since the number of water atoms in the gray matter is distinctly greater than in the white matter (Bottomley et al., 1984). A crucial issue in the present study is the extent to which MRI pixel gray scale distributions distinguish between the brain's gray and white matter in TBI versus control subjects. However, the results of the present study indicate that the MRI distinction between gray matter and white matter is less in brain-injured individuals than in normals, which is consistent with reported visual examinations of MRI scans in TBI patients (Groswasser et al., 1987). The finding of increased number and a widening distribution of intermediate intensity pixels in TBI patients also cannot be explained by partial volume effects or machine parameter differences. Thus, it follows that the constitution of brain tissue is different between the TBI patients and the normal control subjects, which is reflected in an MRI pixel intensity change (PIC). The finding of a gray matter and white matter PD and T2 pixel intensity shift relative to muscle further supports this conclusion.

Limitations of This Study

One of the most notable limitations of a histogram approach to quantitative MRI is the fact that pixel intensity distributions are, to some extent, dependent on machine parameters, such as magnet strength, pulse sequences, signal-to-noise, field of view, etc. In the present study a number of steps were taken to minimize machine-dependent effects and to compare intermachine differences. Normalization of the absolute value of pixel intensity between machines and subjects was accomplished by a Z transform; a ± 4 SD pixel distribution limit helped minimize extraneous or noisy values (Brandt et al., 1994) and statistical analyses were performed to compare TBI patients and normals acquired by two different MRI machines. Normalization of pixel intensity shifts using a common tissue reference such as muscle was also used to control for possible MRI machine differences. Another limitation of this study is the exclusive reliance on proton density and not T1 and/or T2. Proton density was studied because the goal was to compare differences in gray and white matter pixel distributions and proton density is one of the best pulse sequences to distinguish between gray and white matter (Clarke et al., 1995) and it is the least dependent on MR machine parameters (Bottomley et al., 1984; Elster, 1988). Although it is generally agreed that T2-weighted and T2*-weighted images are more sensitive to injury, the present analysis is concerned with subtle changes in the distribution of the gray and white matter pixel intensities. These

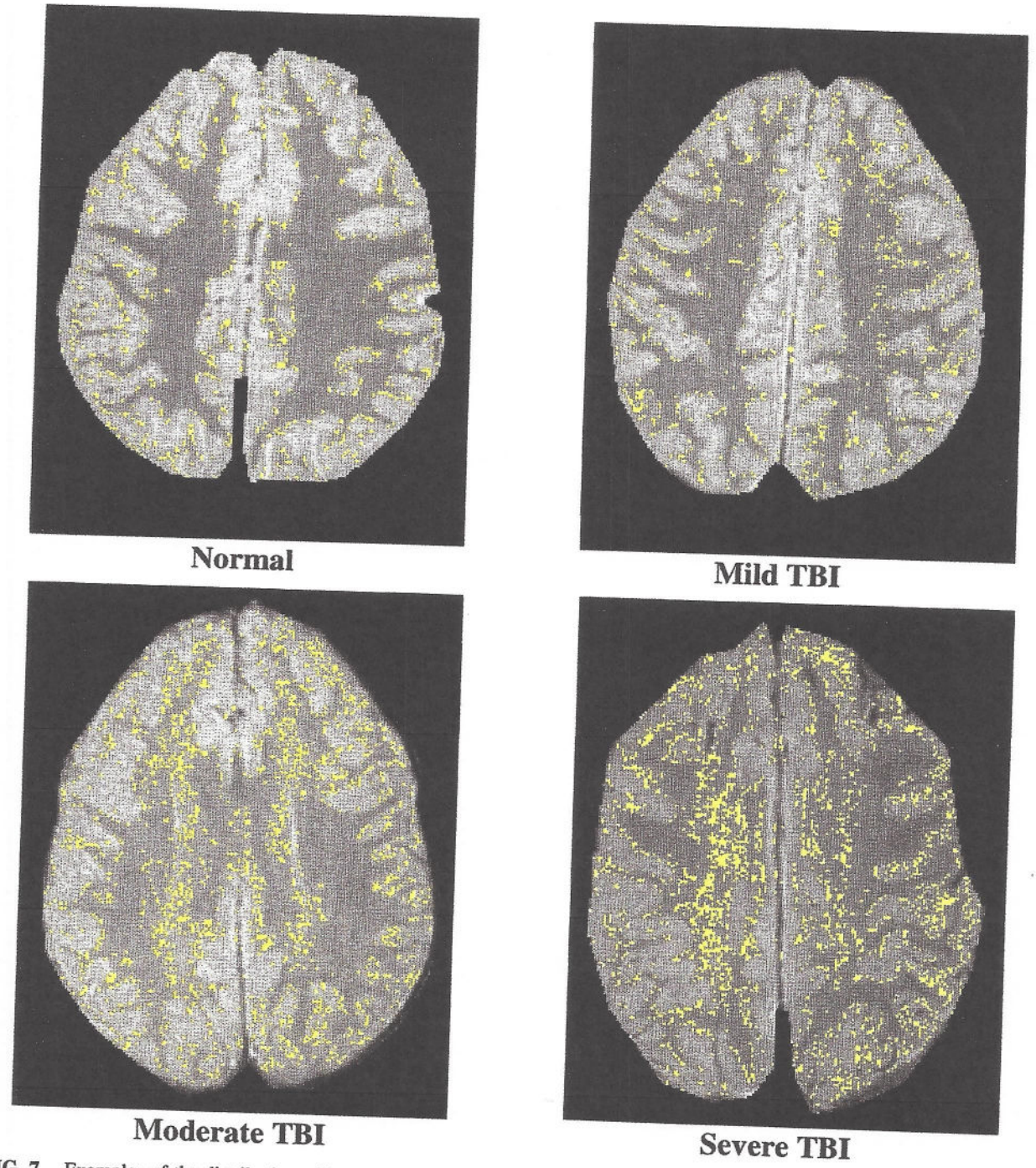

FIG. 7. Examples of the distribution of intermediate pixels, midway between the gray and white matter proton density peaks, which were colored as yellow pixels. The yellow pixels are shown in a normal subject, a mild TBI patient, a moderate TBI patient, and a severe TBI patient.

changes, as our analyses indicate, may actually be quantitatively significant without qualitative signs of injury such as T2 hyperintensities. Finally, regression analyses failed to reveal a statistically significant relation between PIC and the interval of time between injury and MRI test. Thus, the PIC reported in this paper appears to reflect a "chronic" or long-term effect of brain injury and not an acute effect such as edema.

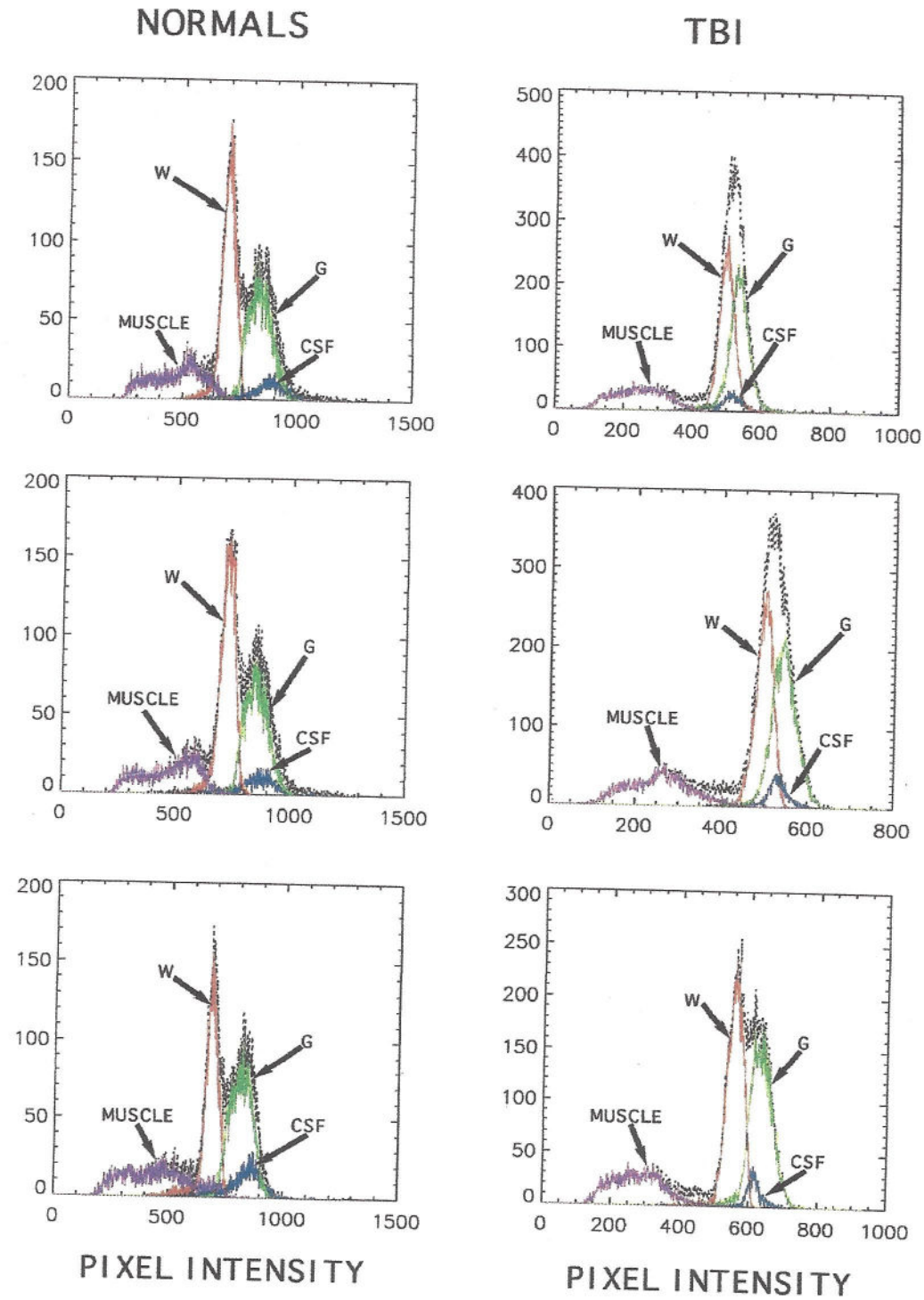

FIG. 8. Examples of pixel intensity distributions in three normal subjects (left column) and three severely injured TBI patients (right column) using 5 mm slice thickness and acquired on G.E. Signa MRI machines. The data were obtained using a kNN segmentation of gray matter, white matter, and muscle. A shift toward higher intensities in gray matter and white matter, with respect to muscle, was observed in the TBI patients. White matter tended to shift more than gray matter, resulting in a more unimodal pixel intensity distribution in TBI patients than in normals. W, white matter; G, gray matter; CSF, cerebral spinal fluid; muscle, masseter muscle.

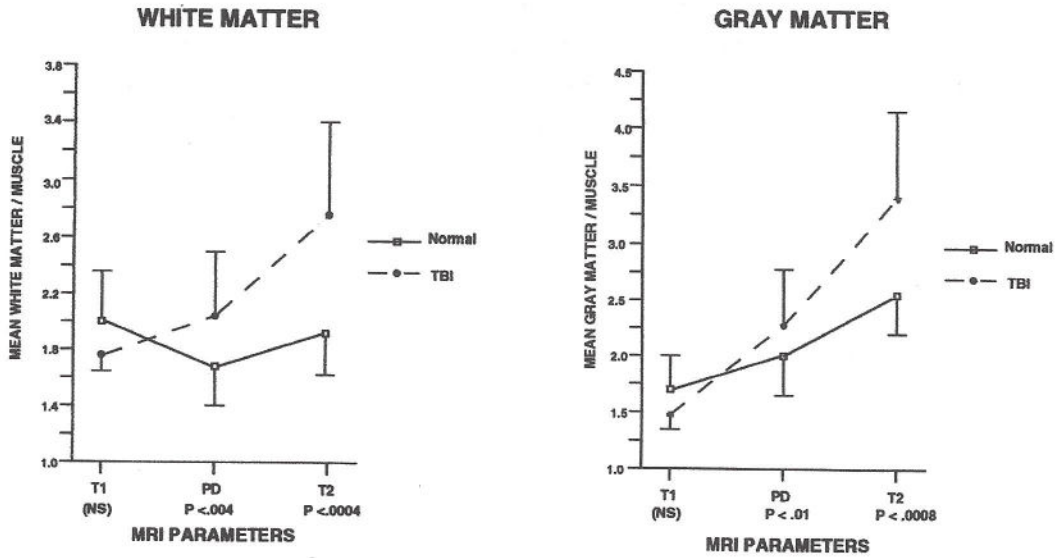

FIG. 9. Mean proton density (PD), T2 and T1 pixel intensity ratios of gray matter and white matter with respect to masseter muscle for the normal controls and TBI patients. Ratios were calculated by dividing the pixel intensities of gray and white matter by the pixel intensity of muscle. Evidence of a pixel intensity shift was provided by statistically significant differences between normal controls and TBI patients in PD and T2. No significant pixel intensity shift with respect to muscle was observed in T1. Error bars represent 1 SD.

Traumatic Brain Injury and Reduced Gray-White Matter Differentiation

A reasonable explanation for the reduced distinction between gray versus white matter in TBI patients is that there is, in fact, reduced tissue differentiation between the gray and white matter due to the consequences of brain injury (Groswasser et al., 1987; Streit and Kincaid-Colton, 1995; Thomas and Steindler, 1995). The exact histological basis for the observed pixel intensity change (PIC), however, is unknown. Studies have shown that TBI results in increased concentrations of microglia, amyloid, phagocytic vacuoles, and other injury products such as extracellular matrix components within both the gray and white matter (Benes et al., 1977; Povlishock et al., 1977; Povlishock and Kontos, 1985; Thomas and Steindler, 1995). Comparisons of gray and white matter pixel intensities with respect to muscle indicated a pixel intensity shift toward higher proton densities and greater T2 relaxation times in TBI patients (Figs. 8 and 9). The reversal of direction and absence of a significant pixel intensity shift in T1 indicates that increased water mobility or increased free water (e.g., as seen by spin-lattice interactions, or T1) cannot explain the differences between normals and TBI patients. Instead increased proton density and T2 spin–spin relaxation times suggest the possibility of increased protein/lipid mobility and/or a new cellular component with different protein and/or lipid water binding properties, such as glia, amyloids, or phagocytic vacuoles. Such changes may be, individually or as a whole, responsible for the reduced differentiation between gray and white matter in TBI patients (Bottomley et al., 1984; Elster, 1988). The widespread and diffuse nature of the observed PIC was examined by coloring the intermediate intensity pixels and displaying them in individual 5-mm and 3-mm slices in normal controls and TBI patients (see Fig. 7). This revealed a progressive increase in the distribution of intermediate intensity pixels as a function of the severity of TBI consistent with the haziness in the border zone observed visually on MRI (Groswasser et al., 1987). In severe TBI patients intermediate pixel intensities were widely distributed within the gray and white matter as well as at the border of the gray and white matter. The distribution of the ambiguous or "fuzzy" set of pixels appeared to reflect a gradient of increased number and distribution of intermediate intensity pixels from mild to severe TBI. This pattern of increased intermediate intensity pixels, when coupled with the finding of increased white matter and gray matter proton density (Figs. 8 and 9), is consistent with the histological findings of Povlishock and Coburn (1989) and others (Streit and Kincaid-Colton, 1995; Thomas and Steindler, 1995) that there is a diffuse increase in glial cells and other reactive products as a function of the magnitude of traumatic brain injury. One possible component of damage contributing to the observed PIC and increasing numbers of intermediate intensity pixels along the gray–white matter boundary

could be DAI. However, the presence of increased numbers of intermediate intensity pixels in the middle of the gray and white matter indicates that a more general biophysical process than DAI alone is responsible for PIC, especially in moderate and severe TBI patients.

ACKNOWLEDGMENTS

We would like to acknowledge the data analysis and editorial assistance of, Alex Ommaya, Rebecca Walker, Karen Gosche, Dr. Irith Reider-Groswasser, Dr. Rebecca McAlaster, and Dr. Robert Velthuizen. This project was supported by contract no. JFC36285006 as part of the Department of Defense and Veterans Head Injury Program (DVHIP).

REFERENCES

ADAMS, J.H, GRAHAM, D.I., MURRAY, L.S., and SCOTT, G. (1982). Diffuse axonal injury due to non-missle head injury. Ann. Neurol. **12,** 257–263.

ADAMS, J.H., DOYLE, D., FORD, I., GENNARELLI, T.A., GRAHAM, D.I., and McLELLAN, D.R. (1989). Diffuse axonal injury in head injury: definition, diagnosis and grading. Histopathology **15,** 49–59.

BENES, F.M., PARKS, T.N., and RUBEL, E.W. (1977). Rapid dendritic atrophy following deafferentation: An EM morphometric analysis. Brain Res **122,** 1–13.

BENSAID, A.M., HALL, L.O., BEZDEK, J.C., and CLARKE, L.P. (1994). Fuzzy cluster validity in magnetic resonance images, in: *Medical Imaging 1994: Image Processing,* M.H. Loew (ed), Proceedings SPIE **2167,** 454–464.

BEZDEK, J.C., HALL, L.O., and CLARKE, L.P. (1993). Review of MR image segmentation techniques using pattern recognition. Med. Phys. **20,** 1033–1048.

BIGLER, E.D., JOHNSON, S., ANDERSON, C., BLATTER, D., GALE, S., RUSSO, A., RYSER, D., MACNAMARA S., and ABILDSKOW, T. (1996). Traumatic brain injury and memory: The role of hippocampal atrophy. Neuropsychology **10**(3), 333–342.

BOTTOMLEY, P.A., FOSTER, T.H., ARGERSINGER, R.E., and PFEIFER, L.M. (1984). A review of normal tissue hydrogen NMR relaxation times and relaxation mechanisms from 1–100 Mhz: Dependence on tissue type, NMR frequency, temperature, species, excision and age. Med. Phys. **11**(4), 425–448.

BRANDT, M.E., BOHAN, T.P., KRAMER, L.A., and FLETCHER, J.M. (1994). Estimation of CSF, white and gray matter volumes in hydrocephalic children using fuzzy clustering of the MR images. Comp. Med. Imag. Graphics **18**(1), 25–34.

CLARKE, L.P., VELTHUIZEN, R.P., CAMACHO, M.A., HEINE, J.J., VAIDYANATHAN, M., HALL, L.O., THATCHER, R.W., and SILBIGER, M.L. (1995). MRI Segmentation: Methods and applications. Magnetic Res. Imaging **13,** 343–368.

ELSTER, A.D. (1988). An index system for comparative parameter weighting in MR imaging. J. Comput. Assis. Tomogr. **12**(1), 130–134.

FRANKOWSKI, R.F., ANNEGERS, J.F., and WHITMAN, S. (1985). Epidemiological and descriptive studies. I. The descriptive epidemiology of head trauma in the United States, in: *Central Nervous System Trauma Status Report.* D.P. Becker and J. Polishock (eds), National Institute of Neurological and Communicative Disorders and Stroke, National Institute of Health: Bethesda, MD, pp. 33–51.

GALE, S.D., JOHNSON, S.C., BIGLER, E.D., and BLATTER, D.D. (1994). Traumatic brain injury and temporal horn enlargement: Correlates with tests of intelligence and memory. Neuropsychiat. Neuropsychol. Behav. Neurol. **7,** 160–165.

GENNARELLI, T.A. (1986). Mechanisms and pathophysiology of cerebral concussion. J. Head Trauma Rehab. **1,** 23–30.

GENNARELLI, T.A., THIBAULT, L.E., ADAMS, J.A., GRAHAM, D.I., THOMPSON, C.J., and MARCINCIN, R.P. (1982). Diffuse axonal injury and traumatic coma in the primate. *Ann. Neurol. 12,* 564–575.

GENTRY, L.R. (1990). Head trauma, *Magnetic Resonance Imaging of the Brain and Spine*, S.W. Atlas (ed), Raven Press, New York, pp. 439–466.

GENTRY, L.R. (1994). Imaging of closed head injury. Radiology **191,** 1–17.

GENTRY, L.R., GODERSKY, J.C., and THOMPSON, B. (1988). MR imaging of head trauma: Review of the distribution and radiopathologic features and traumatic lesions. Am. J. Rad. **150,** 663–672.

GROSWASSER, Z., REIDER-GROSWASSER, I., SOROKER, N., and MACHTEY, Y. (1987). Magnetic resonance imaging in head injured patients with normal late computed tomography scans. Surg. Neurol. **27,** 331–337.

HALL, L.O., BENSAID, A.M., CLARKE, L.P., VELTHUIZEN, R.P., SILBIGER, M.S., and BENDEK, J.C. (1992). A comparison of neural network and fuzzy clustering techniques in segmenting magnetic resonance images of the brain. IEEE Trans. Neural Network. **3,** 672–682.

KWENTUS, J.A., HART, R.P., PECK, E.T., and KORNSTEIN, S. (1985). Psychiatric complications of closed head trauma. Psychosomatics **26,** 8–15.

HOLBOURN, A.H.S. (1943). Mechanics of head injuries. Lancet **2,** 438–441.

HOLBOURN, A.H.S. (1945). The mechanics of brain injuries. Br. Med. Bull. **3,** 147–149.

JOHNSON, S.C., BIGLER, E.D., BURR, R.B., and BLATTER, D.D. (1994). White matter atrophy, ventricular dilation and

intellectual functioning following traumatic brain injury. Neuropsychology **8**(3), 307–315.

POVLISHOCK, J.T. (1986). Traumatically induced axonal damage without concomitant change in focally related neuronal somata and dendrites. Acta Neuropathol **70,** 53–59.

POVLISHOCK, J.T., and COBURN, T.H. (1989). Morphopathological change associated with mild head injury. In: *Mild Head Injury*, H.S. Levin, H.M. Eisenberg, and A.L. Benton (eds), Oxford University Press, New York, pp. 37–53.

POVLISHOCK, J.T., and CHRISTMAN, C.W. (1995). The pathobiology of traumatically induced axonal injury in animals and humans: A review of current thoughts. J. Neurotrauma **12**(4), 555–564.

POVLISHOCK, J.T., and KONTOS, H.A. (1985). Continuing axonal and vascular change following experimental brain trauma. J. Cent. Nervous Syst. Trauma **2,** 285–298.

POVLISHOCK, J.T., BECKER, D.P., CHENG, C.Y., and VAUGHAN, G.W. (1983). Axonal change in minor head injury. J. Neuropathol. Exp. Neurol. **42,** 225–242.

PRAYER, L.M., and GEAN, A.D. (1994). Head trauma, in: *Magnetic Resonance Neuroimaging*, J. Kucharczyk, M. Moselely, and A.J. Barkovich (eds). CRC Press, Boca Raton, pp. 441–478.

PRIGATANO, G.P., and PEPPING, M. (1987). Neuropsychological status before and after mild head injury: A case report. Barrow Neurol. Inst. Quart. **3,** 18–21.

SAVITZKY, A., and GOLAY, M.J.E. (1964). Smoothing and differentiation of data by simplified least squares procedures. Anal. Chem. **36,** 1627–1639.

STREIT, W.J., and KINCAID-COLTON, C.A. (1995). The brain's immune system. Sci. Am. **Nov.,** 54–61.

STRICH, S.J. (1956). Diffuse degeneration of the cerebral white matter in severe dementia following head injury. J. Neurol. Neurosurg. Psychiat. **19,** 163–185.

STRICH, S.J. (1961). Shearing of nerve fibers as a cause of brain damage due to head injury, a pathological study of twenty cases. Lancet **2,** 443–448.

THOMAS, L.B., and STEINDLER, D.A. (1995). Glial boundaries and scars: Programs for normal development and wound healing in the brain. Neuroscientist **1**(3), 142–154.

WEI, E.P., DIETRICH, W.D., POVLISHOCK, J.T., NAVARI, R.M., and KONTOS, H.A. (1980). Functional morphological and metabolic abnormalities of the cerebral microcirculation after concussive brain injury in cats. Circ. Res. **46,** 37–47.

Address reprint requests to:
Robert W. Thatcher, Ph.D.
Research and Development Service—151
Veterans Administration Medical Center
Bay Pines, FL 33744